Optical Materials 32 (2010) 1532–1539

Contents lists available at ScienceDirect

Optical Materials

journal homepage: www.elsevier.com/locate/optmat

Chalcogenide glass hollow core photonic crystal fibers

Frédéric Désévédavy [a,*], Gilles Renversez [b,**], Johann Troles [a], Patrick Houizot [a], Laurent Brilland [c], Ion Vasilief [b], Quentin Coulombier [a], Nicholas Traynor [c], Frédéric Smektala [d], Jean-Luc Adam [a]

[a] Equipe Verres et Céramiques, UMR CNRS 6226, Science Chimiques de Rennes, Université de Rennes I, 35042 Rennes Cedex, France
[b] Institut Fresnel, UMR CNRS 6133, Université d'Aix-Marseille, Av. Escadrille Normandie-Niémen, 13397 Marseille, France
[c] PERFOS, Plate-Forme d'Etude et de Recherches sur les Fibres Optiques Spéciales, 11, rue Louis de Broglie, 22300 Lannion, France
[d] Laboratoire Interdisciplinaire Carnot de Bourgogne, UMR CNRS 5209, Université de Bourgogne, 9 Av. A. Savary, BP 47870, 21078 Dijon cedex, France

ARTICLE INFO

Article history:
Received 22 December 2009
Received in revised form 18 June 2010
Accepted 21 June 2010
Available online 16 July 2010

Keywords:
Chalcogenide glass
Infrared
Photonic crystal fibers
Hollow core
Microstructured optical fibers
Photonic bandgap

ABSTRACT

We report the first hollow core photonic crystal fibers (HC PCF) in chalcogenide glass. To design the required HC PCF profiles for such high index glass, we use both band diagram analysis to define the required photonic bandgap and numerical simulations of finite size HC PCFs to compute the guiding losses. The material losses have also been taken into account to compute the overall losses of the HC PCF profiles. These fibers were fabricated by the stack and draw technique from $Te_{20}As_{30}Se_{50}$ (TAS) glass. The fibers we drew in this work are composed of six rings of holes and regular microstructures. Two profiles are presented, one is known as a kagome lattice and the other one corresponds to a triangular lattice. Geometrical parameters are compared to the expected parameters obtained by computation. Applications of such fibers include power delivery or fiber sensors among others.

1. Introduction

Microstructured optical fibers (MOFs) are a new kind of fiber which have revealed many new properties and also have important potential from an application point of view [1,2]. In a first approach there are two kinds of MOFs: the index guiding ones and the photonic bandgap fibers (PBGFs) also called photonic crystal fibers (PCFs). In PCFs, core localized modes can exist with mode effective indices β/k_0 (where β is the propagation constant and k_0 is the wavenumber in free space) that are lower than the mean index of the microstructured cladding [3,4], so it is possible to guide light in air. Such fibers are called hollow core photonic crystal fibers (HC PCFs). The majority of them have been realized in silica although some HC PCFs are reported in polymer [5–7] and in a polymer chalcogenide combination [8,9]. The last two references deal with Bragg fiber.

There are many reasons for interest in guiding light in a hollow core. For a review of these, see reference [10]. For example, in waveguide-based non-linear optics, HC PCFs can provide strong interaction between the light and the gas which fills the core, allowing a lower energy threshold for Raman amplification [11]. HC PCFs are also of interest for sensors and power delivery [3] and can be used for particle transport [12].

In principle, in HC PCFs losses due to material absorption can be considerably reduced, but silica exhibits such high losses in the mid-infrared [13] that it is not suitable for such wavelengths. Similarly, Omniguide Bragg fibers guiding in a hollow core at 10.6 µm are made of chalcogenide glass and high loss plastic layers [8,9]. Chalcogenide glasses are well known for their transmission window, which extends far in the infrared [13]. They can be drawn to fibers [14] and more recently chalcogenide MOFs have been realized [15,16]. The first chalcogenide MOF with regular microstructure guiding light into the core was obtained at the university of Rennes [16]. The constant improvement of chalcogenide fiber geometry and losses [17–22] has allowed us to fabricate a more complex structure such as an HC PCF. To the best of our knowledge no such results have been published for chalcogenide glasses.

In this article we present the design and realization of the first chalcogenide HC PCF. After the presentation of the simulations we carried out to define the structure parameters, we describe the experimental fabrication and the fabricated fibers. Then characterizations and simulations are compared and the multiple interests of these kinds of fibers discussed.

* Corresponding author.
** Corresponding author.
E-mail addresses: frederic.desevedavy@u-bourgogne.fr (F. Désévédavy), gilles.renversez@fresnel.fr (G. Renversez).
URL: http://www.fresnel.fr/perso/renversez (G. Renversez).

0925-3467/$ - see front matter © 2010 Elsevier B.V. All rights reserved.
doi:10.1016/j.optmat.2010.06.016

2. Design of the target structure

2.1. Infinite structures: band diagram and bandgap

It is worth mentioning that a lot of studies have already been dedicated to the study and to the characterization of HC PCFs made from a silica matrix with an air hole cladding to guide wavelengths around 1.5 μm [23,24,3,25–27]. In the present study, we show how we can design a chalcogenide TeAsSe (TAS) glass HC PCF in which a far infrared beam ($\lambda = 9.3$ μm) can propagate in its hollow core. The guiding of infrared light in HC PCFs has already been studied in a silica PCF but this kind of design [28] is limited to wavelengths below 3.45 μm due to the huge material losses of silica for larger wavelength. Few numerical studies deal with high index HC PCFs [29–32]. None of these considers refractive indices as high as that of TAS glass or designs a PCF for far infrared wavelengths such 9.3 μm like the one obtained in this section. The numerical simulations realized here are done using our own finite element method software which has already been described and carefully validated [4,33]. It is a full vector method that can reach a high accuracy if the spatial discrete mesh used is well adapted. To compute band diagrams [34] with this numerical method, we define periodic boundary conditions in the elementary cell of the triangular lattice of circular inclusions [4].

To ensure propagation in the hollow core, we need to find a bandgap generated by the microstructured cladding that spans the wavelengths of interest where the bandgap must be located below the light line in vacuum (this line corresponds to the dispersion curve of an electromagnetic plane wave in vacuum such that $\beta = k_0$. It is sometimes called the air line) [4]. To obtain this result we compute several band diagrams with the refractive index of the matrix fixed as the value of the TAS glass at 9.3 μm, i.e. $n_{mat} = 2.9095$ [14]. Fig. 1 shows such diagrams computed for three different values of the d/Λ ratio, d being the hole diameter and Λ the pitch of the hole lattice. The bandgap that fulfills the above requirements is shaded. In order to define the more useful bandgap, that is to say the one that will provide the lowest losses for the finite structures, we must study the relative width of this bandgap according to the d/Λ ratio [29,31,32]. The results are given in Fig. 2. We chose $d/\Lambda = 0.775$ because this ratio ensures a large relative width. We picked this value, located on the right side of the relative width maximum plateau, to avoid the rapid decrease observed on the left part of the relative width curve so as to optimize the parameters according to drawing constraints.

For this d/Λ ratio, the centre of the bandgap of interest is located at $\Lambda/\lambda = 0.6925$. Consequently, for $\lambda = 9.3$ μm, the pitch Λ must be set to 6.44 μm. The diameter of the air holes must be equal to 4.991 μm to get the optimal d/Λ ratio. We must emphasize that we are fully aware that these values are much more accurate than those can be reached during the fabrication process but they are the targeted parameters.

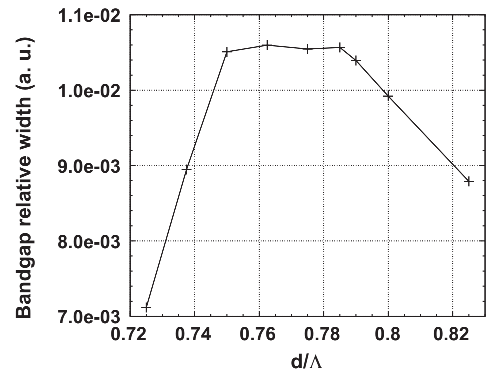

Fig. 2. Relative width of the main bandgap (the shaded region in Fig. 1) around $n_{eff} = 1$ as a function of the normalized air hole diameter d/Λ.

2.2. Finite structures

2.2.1. Guiding losses

To compute the modal properties of finite size MOFs with circular holes, we use the well-known multipole method which is fully vectorial [35,4]. In most microstructured optical fibers, including photonic crystal ones, the modes are leaky modes, it means that the imaginary part of the effective indices is not equal to zero as in genuine guided modes [36,4]. For the above mentioned configurations, the multipole method has the highest possible accuracy since an important part of the method is based on analytical formulas. It can reach an accuracy of 10^{-14} in the real part of the effective index of the mode of simple MOFs and approximatively the same for the imaginary part. With some improvements, even better results can be obtained for the imaginary part [4]. Furthermore, with this method we can define a self-consistency test based on the Wijngaard expansion [4,35] that allows us to control the accuracy of the computed solution. The losses of finite size silica HC PCFs has already been computed with the multipole method [26,4]. These losses, $\mathscr{L}$ in dB/m, can be computed from the imaginary part of the complex effective index $\Im m(n_{eff})$ of the studied mode using the following formula in which λ is in μm [4]:

$$\mathscr{L} = \frac{20}{\ln(10)} \frac{2\pi}{\lambda} \Im m(n_{eff}) \times 10^6 \quad (1)$$

It appears that for fixed values of d and Λ determined by the choice of the bandgap used, the minimal value of the losses as a function of the wavelength inside the bandgap decreases nearly exponentially with the number of hole rings N_r of the microstructured cladding of the HC PCF [4].

2.2.2. Influence of the core diameter

It is well known from previous studies [37,38,28,32] based on silica PCFs that the core size and shape are key parameters for

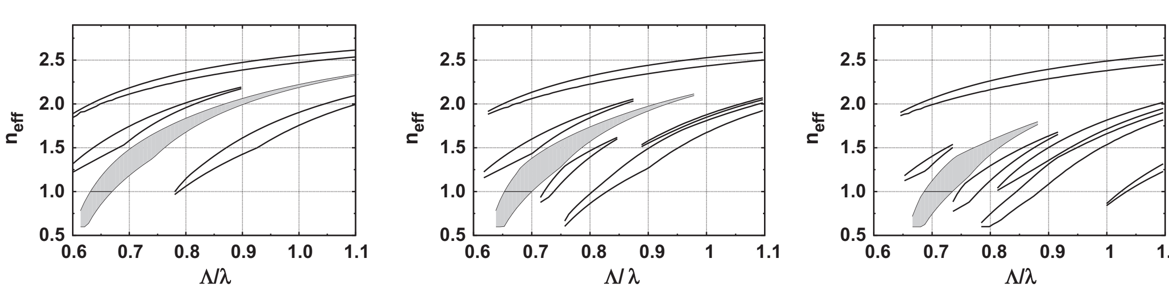

(a) $d/\Lambda = 0.7375$ (b) $d/\Lambda = 0.7625$ (c) $d/\Lambda = 0.79$

Fig. 1. Band diagrams obtained for three triangular lattices of circular air holes in a TAS matrix such that $n_{mat} = 2.9095$. The shaded region is the bandgap of interest. ($n_{eff} = \beta/k_0$).

the modal properties of finite structures due to the impact of surface modes [39]. In order to determine the optimal value of the core diameter D_{core}, we compute the dispersion curves of finite size fibers for several core sizes up to a core corresponding to seven missing capillaries. For $D_{core} = 12.58$ µm, we obtain fundamental mode losses that are nearly four times smaller than the ones from other configurations. We also observe that the shape of the field map depends strongly on the core diameter. At least for the optimal D_{core} value, these results can be explained quantitatively (if not perfectly) using the simplified ARROW model Anti-Resonant Reflecting Optical Waveguides [40]. In the HC PCF studied, the ARROW confinement allows better confinement of the core modes that are already confined by the cladding due to the existing photonic bandgap.

Indeed, if one considers a slab of thickness e with a low refractive index denoted by n_{low} as the waveguide, covered by a layer of thickness t with a high refractive index n_{high}, then the anti-resonant condition for a guided wave with wavelength λ in the low index layer determines the discrete values of t, denoted by t^*, ensuring the confinement of the mode [40]:

$$t^* = \lambda(2m+1)/\left(4n_{high}\sqrt{1-\frac{n_{low}^2}{n_{high}^2}+\frac{\lambda^2}{4n_{high}^2 e^2}}\right) \quad \text{with} \quad m = 0,1,2,3,\ldots \tag{2}$$

To adapt this mode to a circular hollow core PCF, we can consider that the thickness e is equal to $D_{core}/2$, together with $n_{low} = n_{air}$ and $n_{high} = n_{mat}$. The high index ring around the core will acts as the anti-resonant layer. Consequently, for a PCF with a fixed d/Λ ratio, the core diameter sets the thickness t of the high index ring through the relation:

$$t = 2\Lambda - \frac{d}{2} - \frac{D_{core}}{2} \tag{3}$$

Combining Eq. (2) with the already mentioned approximation $e = D_{core}/2$ and Eq. (3) we get a non-linear equation that allows us to compute the core diameters fulfilling the anti-resonant condition. For the optogeometric parameters obtained previously, we get $D_{core} = 15.69$ µm $(m = 1)$ and $D_{core} = 12.34$ µm $(m = 2)$. As it will be seen in the next paragraph and in Fig. 3, the ARROW model gives valid quantitative results in spite of the crude approximations made to move from the PCF to the slab.

To complete these results, we can also compute the dispersion curves of the fundamental mode in order to find the minimal losses and their respective wavelengths (see Fig. 3). Fig. 3 confirms that the influence of the core diameter is crucial: both the loss minimum and its wavelength are very sensitive to its value. It also shows that the core diameter range in which both low guiding losses and a wavelength around the targeted 9.3 µm are achieved is between 12.58 µm and 13.08 µm. The second interesting interval for the core diameter is around 15.33 µm but the guiding losses are higher than the ones computed for $D_{core} \simeq 13$ µm (see Fig. 3). Consequently, this second configuration would require more rings of holes to get the same low losses compared to the first one (data not shown). Therefore, this second configuration was not selected for the optimization procedure.

Using the computed losses, we can evaluate the spectral width of the PCF transmission as a function of the core diameter. Two definitions of the spectral width are used: a relative one defined as an increase of 10% of the losses compared to the minimum and an absolute one defined as an increase of 10 dB. These results (Fig. 4) clearly show the advantage of using an optimized value for the core diameter. The physical origin of the upper wavelength cutoff of this transmission window is discussed at the end of the next paragraph though with regard to an optimized structure.

2.3. An optimized structure

We now set the core diameter to the central value, i.e. 12.83 µm, of the above selected interval. To optimize further the guiding properties of the fiber, we need to readjust the other structure parameters Λ and d so as to get the losses minimum exactly at 9.3 µm. To realize this we must diminish Λ, keeping the d/Λ ratio equal to 0.775. A simple rule of three gives $\Lambda = 6.41$ µm and finally we get $d = 4.968$ µm.

With this structure, the fundamental mode field map (see Fig. 5) does not have a circular shape like in Fig. 7.28 of reference [4] but rather an elliptical one. We obtain the fundamental mode dispersion curves shown Fig. 6. As expected, the real part of the effective index $\Re e(n_{eff})$ does not depend on the number of rings of holes, N_r, whereas the losses decreases nearly exponentially with N_r [4]. The losses of this mode at 9.3 µm for several N_r values are given in the left side of Table 1 for a lossless matrix. As soon as $N_r > 6$ the losses are less than 1 dB/m. This level is nearly three times lower than the losses measured at 3.14 µm with a silica-based PCFs [28]. Nevertheless, in order to improve our fiber model, we can take into account the material losses of the TAS glass. The measured material attenuation is 1.5 dB/m at 9.3 µm which provides a relative

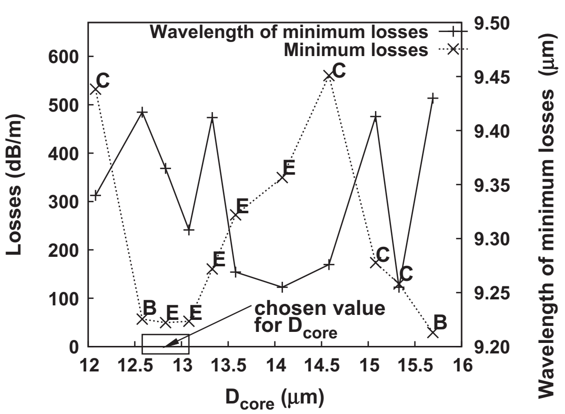

Fig. 3. Guiding losses (left axis, dashed curve) as a function of the core diameter D_{core} for HC PCFs with four rings of holes ($N_r = 4$), $\Lambda = 6.44$ µm, $d = 4.991$ µm. The letters *B*, *C*, and *E* indicate the shape of the modulus of the *z*-component of the Poynting vector for the fundamental mode: *B* for a bi-lobe shape, *C* for a centro-symmetrical one and *E* for an elliptical one. The wavelength of the minimal losses as a function of D_{core} are given on the right axis (solid curve).

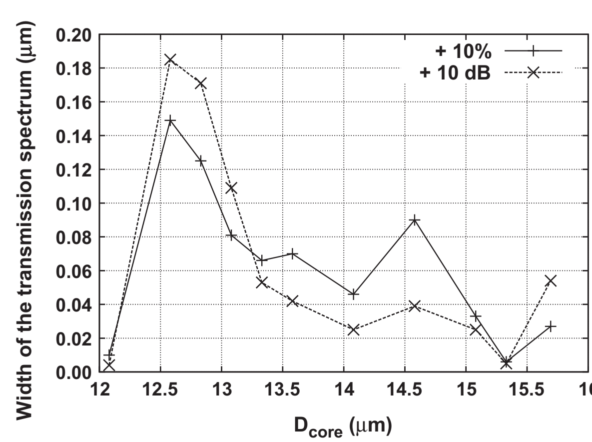

Fig. 4. Width of the transmission spectrum of the HC PCF as a function of the core diameter. Two definitions of the width are used: a relative one defined as an increase of 10% of the losses compared to the minimum and an absolute one defined as an increase of 10 dB.

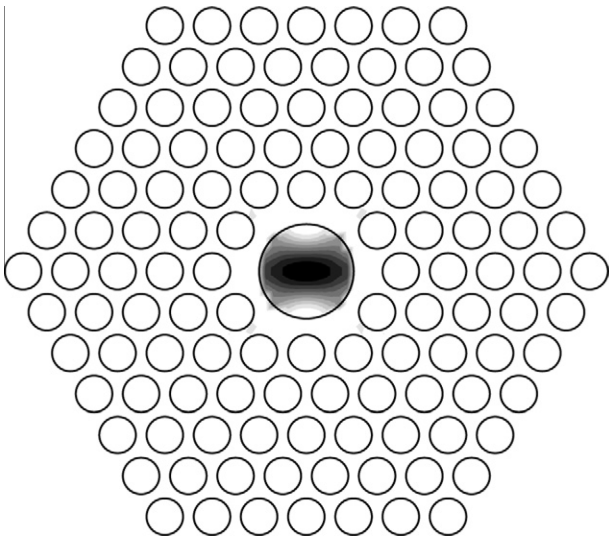

Fig. 5. Modulus of the z-component of the Poynting vector for the fundamental mode of the HC PCF $N_r = 5$ for $D_{core} = 12.83$ µm, $\Lambda = 6.41$ µm and $d = 4.968$ µm. The modulus is normalized to unity.

imaginary electric permittivity equal to 1.49×10^{-6}. The corresponding results are given in the right side of Table 1. We see that the overall losses of the fundamental mode are below the material losses for $N_r \geqslant 6$ since most of the electromagnetic fields are confined in the hollow core and not in the glass matrix. For $N_r = 7$ these losses are nearly five times smaller than those of the silica PCF mentioned in ref. [28]. The anti-resonant phenomenon described above is also responsible for the elliptic shape of the field map observed on Fig. 5 (one can note that the bi-lobe shape field map (see the legend of Fig. 3) corresponds to an increase of the field in the core near the border of the high index region as can be seen in the original ARROW model [40]).

It is worth noting that an example of surface mode interaction with the air-core localized mode guided by photonic bandgap effect can be observed in Fig. 6(a). The dispersion curve of the leaky mode has an important slope change around the mid-bandgap (around 9.42 µm), due to an avoided crossing with a surface leaky mode of the matrix region surrounding the core. In the weak slope region, the mode is core localized. Then for longer wavelengths it rapidly moves to the high index glass ring surrounding the hollow core (see Fig. 7) where it has both a much higher dispersion slope and higher losses. This phenomenon is well known and has already

Table 1
Losses of the fundamental mode of the HC PCF at 9.3 µm for several values of the number of rings of holes N_r.

N_r	Without material losses		With material losses	
	$\Im m(n_{eff})$	Losses (dB/m)	$\Im m(n_{eff})$	Losses (dB/m)
3	$0.99669946E{-}04$	584.89	$0.99763273E{-}04$	585.439
4	$0.83702342E{-}05$	49.115	$0.84636519E{-}05$	49.667
5	$0.10102266E{-}05$	5.928	$0.11036755E{-}05$	6.476
6	$0.927366E{-}07$	0.544	$0.18618142E{-}06$	1.092
7	$0.100995E{-}07$	0.059	$0.1035440E{-}06$	0.607

The fiber parameters are: $\Lambda = 6.41$ µm, $d = 4.968$ µm, and $D_{core} = 12.83$ µm. The material losses (1.5 dB/m) are taken into account through a relative imaginary electric permittivity fixed at 1.49×10^{-6}.

been observed among various structures such as Bragg MOFs [41], HC PCFs [39] and ARROW MOFs in which a core localized mode transition towards high index regions can be observed in the Fig. 2 of reference [42]. Especially for PCFs, it limits the useful bandwidth where core localized modes have low loss. For our optimized structure, as it can be seen in Fig. 6(b), the spectral range centered around 9.3 µm where the guiding losses are less than 1 dB/m is approximately 0.2 µm.

Finally, the computed parameters for HC PCF allowing guiding of light in air at 9.3 µm are shown in Table 2.

3. HC PCF fabrication

We selected the TAS glass because of its high infrared transparency [14] (Fig. 8). The nominal composition of the chalcogenide glass we studied is $Te_{20}As_{30}Se_{50}$ (TAS), it is transparent between 2 µm and 20 µm, and its refractive index varies from 2.96 at 2 µm to 2.90 at 12 µm [14,43]. The glass fabrication method is described in [44].

The microstructured preform was prepared by stack and draw technique, replacing the seven capillaries (the core and the first ring) of the centre by a single bigger one. The chalcogenide glass capillaries for the cladding and the core, were obtained by tube drawing. A TAS glass tube was made by rotational casting. During this operation the glass was melted at 500 °C, centrifuged at 3000 rpm at room temperature for several minutes and then annealed. During rotation, the liquid cools down, the viscosity increases and after a few minutes the glass tube formed. In this case the tube dimensions were 17 cm × 1.2 cm × 0.9 cm (length × outer diameter × inner diameter).

The hollow core PCFs in TAS glass we present here are made of six hole rings and fabricated by the stack and draw technique

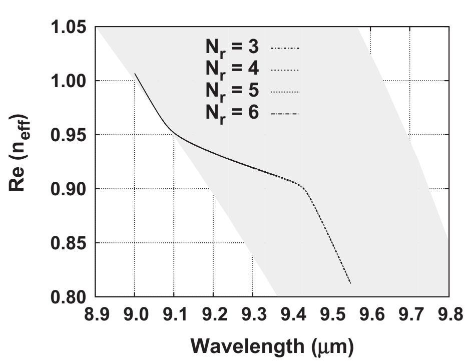

(a) $\Re e\,(n_{eff})$

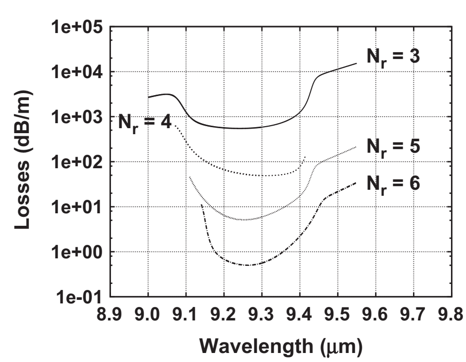

(b) Losses (dB/m)

Fig. 6. Dispersion curves of the fundamental mode of the PCF for several number of hole rings N_r. $D_{core} = 12.83$ µm, $\Lambda = 6.41$ µm, $d = 4.968$ µm. The dispersion curves (left graph) for $N_r = 3, 4, 5, 6$ are fully superimposed at this scale. One can note that these four curves have an important slope change around the mid-bandgap, it is due to an avoided crossing with a surface mode of the matrix region surrounding the core. The shaded area on the left graph represents the main photonic bandgap obtained in Fig. 1.

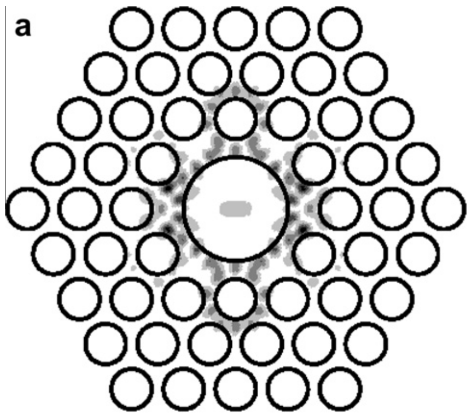

Fig. 7. Modulus of the z-component of the Poynting vector for the surface mode of the HC PCF in the high slope region of the dispersion curve shown in Fig. 6 (a) at two different wavelengths (note the remaining weak field in the hollow core at $\lambda = 9.45$ μm). $N_r = 3$, $D_{core} = 12.83$ μm, $\Lambda = 6.41$ μm and $d = 4.968$ μm. The modulus is normalized to unity. (a) $\lambda = 9.45$ μm, (b) $\lambda = 9.5$ μm.

Table 2
Summary of the calculated theoretical HC PCF parameters for a guiding at 9.3 μm, and data of the preform and of the two fabricated fibers.

Parameters	Computed optimum for guiding (μm)	Preform (μm)	Hexagonal fiber (μm)	Kagome fiber (μm)
d	[4.935, 5.065]	450	8.7	17.6
Λ	6.41	600	12.1	23.8
d/Λ	[0.77, 0.79]	0.75	0.72	0.74
Φ_{core}	At least 12.1 best at 12.83	1350	32	57.8
Φ_{fiber}	Not applicable	12,000	225	425

Φ_{core} is the core diameter. Φ_{fiber} is the outer fiber diameter.

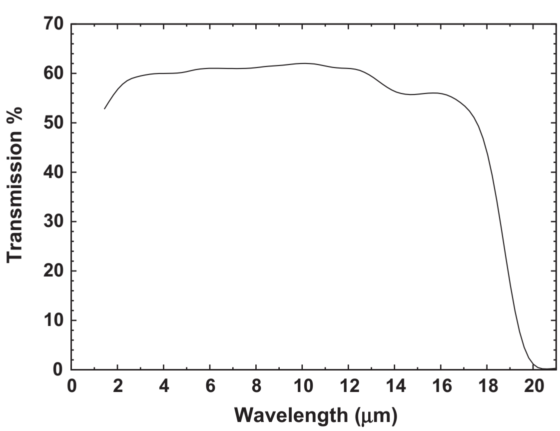

Fig. 8. TAS transmission window measured on a bulk sample 2.26 mm thick.

which is compatible with chalcogenide glasses [16]. In order to prepare the 162 capillaries, necessary for this six ring preform, the tube is drawn on our drawing tower at 260 °C. Capillary dimensions were 600 μm × 450 μm (outer diameter × inner diameter), the starting pitch of this preform, i.e. the distance between two adjacent capillary centers, is then equal to 0.75 which is already close to the targeted one defined by simulations (between 0.77 and 0.79) see Table 2.

Previous experiments with fewer rings taught us that, because the seven capillaries of the centre are replaced by a single large one (for this design), the stack needs to be stabilized. To achieve this, we used a core capillary with an external hexagonal shape.

Fig. 9. Hexagonal tube in TAS glass which has been drawn to obtain the core capillary. The maximum outer diameter (between two opposite vertices) of this capillary is 1.8 mm, its inner diameter is 1.35 mm.

This core was prepared from a tube on which six identical faces are polished, the angle between each pair of adjacent faces is 120 °C. An image of this hexagonal tube is shown in Fig. 9. This special tube was then drawn down to a capillary. The outer diameter of this core tube was three times the outer diameter of one of the smaller capillaries used to form the cladding as shown in Fig. 10. As this preform drawing is a homothetic process the capillary resulting from the hexagonal tube is also hexagonal. The maximal outer length of this core capillary was 1.8 mm between two opposite vertices, while the inner diameter of the tube was 1.35 mm.

In a next step, the 162 capillaries and the hexagonal core were stacked together in a hexagonal lattice and placed in a larger jacket tube to create the preform.

During the fiber drawing process, the integrity of the structure was preserved by independently pressurizing the core, the cladding, and the region separating the jacket tube from the stack, as it is illustrated in Fig. 10. We use three independent pressures, P_1 in the core, P_2 in the holes and P_3 in the interstices between holes and between stack and jacket. P_3 can be either positive or negative. For the kagome fiber, the interstices are intentionally open, i.e. we put positive pressure in the interstices to open them (it is not due

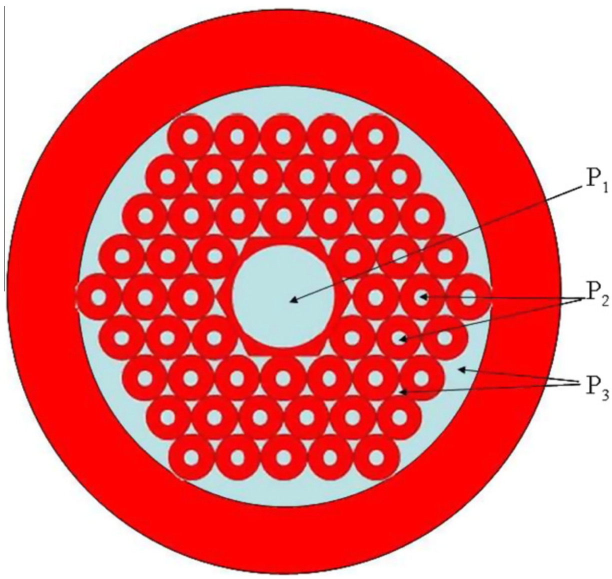

Fig. 10. Scheme of a three ring stack with an hexagonal core, in its jacket tube. The P_i (i = 1, 2, 3) are the different pressure regions used during the drawing (see the text).

to incomplete drawing). On the contrary, for the hexagonal fiber, we use vacuum for interstices to close themselves.

4. Results and discussion

The geometrical parameters allowing guiding in air at 9.3 μm, resulting from modeling, are gathered in the Table 2.

Fig. 11 shows the transverse cross sections of the two six ring TAS glass HC PCFs which we have fabricated. One can observe that the geometry is quite well defined, the six rings are regular, and the interstitial holes too. The average length of their sides is 6 μm. In comparison with the hexagonal cladding lattice of the fiber in Fig. 11(a), the fiber in Fig. 11(b), with the interstitial holes, presents an alternative hollow core fiber design. This cladding structure where the repeating unit is a "Star of David" shape is called a kagome lattice, and shows broad transmission regions at least in silica HC PCFs [45]. To the best of our knowledge, these two fibers are the first HC PCFs fabricated in chalcogenide glass.

The regularity of these chalcogenide HC PCFs is comparable with polymer ones [5] and even with silica ones [3,11]. The interstitials holes can be closed or opened depending of the pressure conditions. With negative pressure the interstitial holes tend to close up like in Fig. 11(a), on the contrary with positive pressure they expand, as in Fig. 11(b). In both fibers the hole size is regular and they are all present, except for some holes of the sixth ring of the hexagonal fiber which are a little squashed (see Fig. 11(a)). Concerning the fiber parameters given in Table 2, one must keep in mind that fiber and hole diameters are not exactly linearly related to those of the preform because of the pressure conditions we use (see Fig. 10). Indeed, it makes this kind of drawing a non-homothetic process. In other respects, one has to know that for the whole process, i.e. from the glass fabrication to the HC PCF preform preparation and its drawing, several weeks of work are necessary.

In the case of hollow core, the interface problem between adjacent capillaries we met with solid core fiber [22] will have a little impact on the optical losses because the light is supposed to be mostly guided in the air. However because of an experimental problem, related to the airtightness of the preform, we did not achieve the targeted geometrical parameters for a guiding at 9.3 μm in the hollow core. Unfortunately, the targeted HC PCF profile was not reached and no propagation was observed in the core fibers between 2 and 20 μm. Nevertheless the proportions are quite close to the theoretical ones, as illustrated by the ratio d/Λ (see Table 2). This means that our fabrication process may allow us to realize HC PCF with the targeted geometrical parameters for guiding in air at 9.3 μm or at 10.6 μm. To achieve this result, we must be able to increase the d/Λ ratio by less than 7% for the hexagonal cladding fiber, and above all to decrease the transverse length scale of the fiber by a factor around 2.

It is worth mentioning that we have developped a new fabrication process for chalcogenide glasses based on molding that allows us to draw several kinds of low loss solid core MOFs [46]. In the future, this method could be extented to chalcogenide HC PCFs.

The core wall thickness of the fiber shown in Fig. 11(b) varies from 3 to 10 μm, taking into account the thickness of the central capillary added to the ones of the cladding capillaries around it. This large thickness is prejudicial for guiding since it is favourable to defect modes that interact with the core localized mode [47,48]. We believe it is possible to decrease the wall thickness of the core by removing the hexagonal core capillary from the stack in the useful length of the HC PCF. We plan to use only two short hexagonal

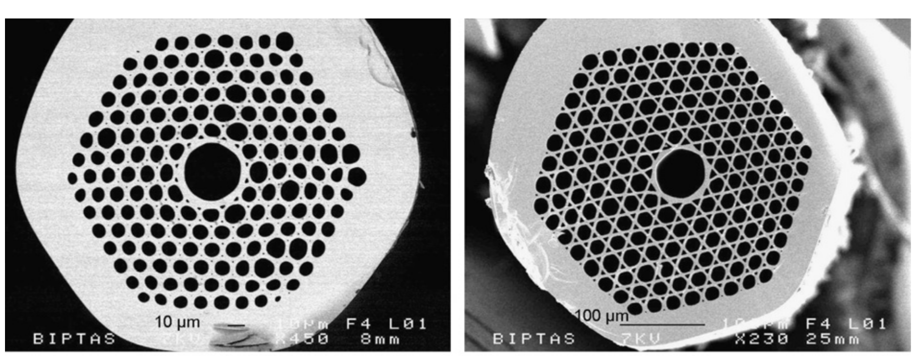

(a) with hexagonal lattice cladding : fiber diameter = 225 μm, Λ = 12.1 μm, d = 8.7 μm, d/Λ = 0.72, Φ_{core} = 32 μm.

(b) with kagome lattice cladding : fiber diameter = 425 μm, Λ = 23.8 μm, d = 17.6 μm, d/Λ = 0.74, Φ_{core} = 57.8 μm, triangle sides = 6.0 μm.

Fig. 11. TAS hollow core PCF profiles. Φ_{core} is the core diameter.

core capillaries at both ends of the preform to maintain the stack instead of a full length one like we did. The airtightness would be made by a jacketing step. Then the preform will be drawn using the three independent pressures system we used for the fibers presented here. In this way we could control the opening and closing of the interstices. Another challenge, is to improve the regularity of the hole shape, this will be done by a better control on the tube drawing and by drastic diameter selection of the resulting capillaries.

5. Conclusion

We have designed the first hollow core photonic crystal fiber made of chalcogenide TAS glass to guide light in its core at 9.3 μm. We have optimized both the cladding structure and the core size to lower the losses. The computed overall losses of the optimized HC PCF, including the 1.5 dB/m bulk TAS glass ones, are around 1 dB/m at 9.3 μm for six rings of hole inclusions and only slightly above 0.6 dB/m at the same wavelength for seven rings of holes. The two first hollow core fibers in chalcogenide glass with a 2D photonic crystal cladding, potentially guiding light at 9.3 μm have also been realized. Indeed we fabricated two fibers with a sufficient number of rings for overall losses to be less than material ones i.e. six rings and with a regular geometry. The next challenge is to reach the predicted geometrical parameters, to allow infrared guiding in air. To reach this objective we plan to improve our process to avoid airtightness anomalies and to decrease the core's walls thickness. Indeed, the realization of chalcogenide photonic bandgap fiber represents a technological challenge.

Acknowledgments

We acknowledge the French Délégation Générale pour l'Armement (Contracts 05.43.053 and 07.34.031) for its financial support.

References

[1] P. Kaiser, E.A.J. Marcatili, S.E. Miller, A new optical fiber, Bell Syst. Tech. J. 52 (1973) 265–269.
[2] P.St.J. Russell, Photonic crystal fibers, Science 299 (5605) (2003) 358–362.
[3] R.F. Cregan, B.J. Mangan, J.C. Knight, T.A. Birks, P. St. Russell, P.J. Roberts, D.C. Allan, Single-mode photonic band gap guidance of light in air, Science 285 (5433) (1999) 1537–1539.
[4] F. Zolla, G. Renversez, A. Nicolet, B. Kuhlmey, S. Guenneau, D. Felbacq, Foundations of photonic crystal fibres, Imperial college Press, 2005.
[5] A. Argyros, J. Pla, Hollow-core polymer fibres with a kagome lattice: potential for transmission in the infrared, Opt. Express 15 (12) (2007) 7713–7719.
[6] A. Argyros, M.A. van Eijkelenborg, M.C. Large, I.M. Bassett, Hollow-core microstructured polymer optical fiber, Opt. Lett. 31 (2) (2006) 172–174.
[7] B. Gauvreau, N. Guo, K. Schicker, K. Stoeffler, F. Boismenu, A. Ajji, R. Wingfield, C. Dubois, M. Skorobogatiy, Color-changing and color-tunable photonic bandgap fiber textiles, Opt. Express 16 (20) (2008) 15677–15693.
[8] A.F. Abouraddy, M. Bayindir, G. Benoit, S.D. Hart, K. Kuriki, N. Orf, O. Shapira, F. Sorin, B. Temelkuran, Y. Fink, Towards multimaterial multifunctional fibres that see, hear, sense and communicate, Nat. Mater. 6 (5) (2007) 336–347.
[9] B. Temelkuran, S.D. Hart, G. Benoit, J.D. Joannopoulos, Y. Fink, Wavelength-scalable hollow optical fibres with large photonic bandgaps for CO_2 laser transmission, Nature 420 (6916) (2002) 650–653.
[10] F. Benabid, Hollow-core photonic bandgap fibre: new light guidance for new science and technology, Phil. Trans. R. Soc. A 364 (1849) (2006) 3439–3462.
[11] F. Benabid, J.C. Knight, G. Antonopoulos, P.St.J. Russell, Stimulated raman scattering in hydrogen-filled hollow-core photonic crystal fiber, Science 298 (5592) (2002) 399–402.
[12] F. Benabid, J.C. Knight, P.S.J. Russell, Particle levitation and guidance in hollow-core photonic crystal fiber, Opt. Express 10 (21) (2002) 1195–1203.
[13] X.H. Zhang, B. Bureau, P. Lucas, C. Boussard-Pledel, J. Lucas, Glasses for seeing beyond visible, Chem. A Eur. J. 14 (2) (2008) 432–442.
[14] P. Houizot, C. Boussard-Pledel, A.J. Faber, L.K. Cheng, B. Bureau, P.A. Van Nijnatten, W.L.M. Gielesen, J.P. do Carmo, J. Lucas, Infrared single mode chalcogenide glass fiber for space, Opt. Express 15 (19) (2007) 12529–12538.
[15] T.M. Monro, Y.D. West, D.W. Hewak, N.G.R. Broderick, D.J. Richardson, Chalcogenide holey fibres, Electron. Lett. 36 (24) (2000) 1998–2000.
[16] L. Brilland, F. Smektala, G. Renversez, T. Chartier, J. Troles, T.N. Nguyen, N. Traynor, A. Monteville, Fabrication of complex structures of holey fibers in chalcogenide glass, Opt. Express 14 (3) (2006) 1280–1285.
[17] F. Désévédavy, G. Renversez, J. Troles, L. Brilland, P. Houizot, Q. Coulombier, F. Smektala, N. Traynor, J.-L. Adam, Te–As–Se glass microstructured optical fiber for the middle infrared, Appl. Opt. 48 (19) (2009) 3860–3865.
[18] F. Désévédavy, G. Renversez, L. Brilland, P. Houizot, J. Troles, Q. Coulombier, F. Smektala, N. Traynor, J.-L. Adam, Small-core chalcogenide microstructured fibers for the infrared, Appl. Opt. 47 (32) (2008) 6014–6021.
[19] C. Fortier, J. Fatome, S. Pitois, F. Smektala, G. Millot, J. Troles, F. Désévédavy, P. Houizot, L. Brilland, N. Traynor, Experimental investigation of brillouin and raman scattering in a 2SG sulfide glass microstructured chalcogenide fiber, Opt. Express 16 (13) (2008) 9398–9404.
[20] F. Smektala, F. Désévédavy, L. Brilland, P. Houizot, J. Troles, N. Traynor, Advances in the elaboration of chalcogenide photonic crystal fibers for the midinfrared, Proc. SPIE 6588 (2007) 658803.
[21] J. Troles, L. Brilland, F. Smektala, P. Houizot, F. Désévédavy, Q. Coulombier, N. Traynor, T. Chartier, T.N. Nguyen, J.L. Adam, G. Renversez, Chalcogenide microstructured fibers for infrared systems, elaboration modelization, and characterization, Fiber Integr. Opt. 28 (2009) 11–26.
[22] L. Brilland, J. Troles, P. Houizot, F. Désévédavy, Q. Coulombier, G. Renversez, T. Chartier, T.N. Nguyen, J.L. Adam, N. Traynor, Interfaces impact on the transmission of chalcogenides photonic crystal fibres, J. Ceram. Soc. Jpn. 116 (1358) (2008) 1024–1027.
[23] T.A. Birks, P.J. Roberts, P.St.J. Russell, D.M. Atkin, T.J. Shepherd, Full 2-d photonic bandgaps in silica/air structures, Electron. Lett. 31 (22) (1995) 1941–1943.
[24] J.C. Knight, J. Broeng, T.A. Birks, P.S.J. Russel, Photonic band gap guidance in optical fibers, Science 282 (5393) (1998) 1476–1478.
[25] S.E. Barkou, J. Broeng, A. Bjarklev, Silica-air photonic crystal fiber design that permits waveguiding by a true photonic bandgap effect, Opt. Lett. 24 (1) (1999) 46–48.
[26] T. White, R. McPhedran, L. Botten, G. Smith, C.M. de Sterke, Calculations of air-guided modes in photonic crystal fibers using the multipole method, Opt. Express 9 (13) (2001) 721–732.
[27] Y. Xu, A. Yariv, Loss analysis of air-core photonic crystal fibers, Opt. Lett. 28 (20) (2003) 1885–1887.
[28] J.D. Shephard, W.N. MacPherson, R.R.J. Maier, J.D.C. Jones, D.P. Hand, M. Mohebbi, A.K. George, P.J. Roberts, J.C. Knight, Single-mode mid-ir guidance in a hollow-core photonic crystal fiber, Opt. Express 13 (18) (2005) 7139–7144.
[29] J.M. Pottage, D.M. Bird, T.D. Hedley, T.A. Birks, J.C. Knight, P.St.J. Russell, P.J. Roberts, Robust photonic band gaps for hollow core guidance in PCF made from high index glass, Opt. Express 11 (22) (2003) 2854–2861.
[30] L.B. Shaw, J.S. Sanghera, I.D. Aggarwal, F.H. Hung, As–S and As–Se based photonic band gap fiber for IR laser transmission, Opt. Express 11 (25) (2003) 3455–3460.
[31] G.J. Pearce, J.M. Pottage, D.M. Bird, P.J. Roberts, J.C. Knight, P.St.J. Russell, Hollow-core PCF for guidance in the mid to far infra-red, Opt. Express 13 (18) (2005) 6937–6946.
[32] J. Hu, C.R. Menyuk, Leakage loss and bandgap analysis in air-core photonic bandgap fiber for nonsilica glasses, Opt. Express 15 (2) (2007) 339–349.
[33] F. Drouart, G.. Renversez, A. Nicolet, C. Geuzaine, Spatial Kerr solitons in optical fibers of finite size cross section: beyond the Townes soliton, J. Opt. A: Pure Appl. Opt. 10 (2008) 125101.
[34] A.A. Maradudin, A.R. McGurn, Out of plane propagation of electromagnetic waves in a two-dimensional periodic dielectric medium, J. Mod. Opt. 41 (2) (1994) 275–284.
[35] B. Kuhlmey, T.P. White, G. Renversez, D. Maystre, L. Botten, C.M. de Sterke, R.C. McPhedran, Multipole method for microstructured optical fibers II: implementation and results, J. Opt. Soc. Am. B 10 (19) (2002) 2331–2340.
[36] A.W. Snyder, J.D. Love, Optical Waveguide Theory, Chapman & Hall, New York, 1983.
[37] K. Saitoh, M. Koshiba, Leakage loss and group velocity dispersion in air-core photonic bandgap fibers, Opt. Express 11 (23) (2003) 3100–3109.
[38] K. Saitoh, N.A. Mortensen, M. Koshiba, Air-core photonic bang-gap fibers: the impact of surface modes, Opt. Express 12 (3) (2004) 394–400.
[39] J. West, C. Smith, N. Borrelli, D. Allan, K. Koch, Surface modes in air-core photonic band-gap fibers, Opt. Express 12 (8) (2004) 1485–1496.
[40] M.A. Duguay, Y. Kokubun, T.L. Koch, L. Pfeiffer, Antiresonant reflecting optical waveguides in $SiO_2 - Si$ multilayer structures, Appl. Phys. Lett. 49 (1) (1986) 13–15.
[41] T.D. Engeness, M. Ibanescu, S.G. Johnson, O. Weisberg, M. Skorobogatiy, S. Jacobs, Y. Fink, Dispersion tailoring and compensation by modal interactions in omniguide fibers, Opt. Express 11 (10) (2003) 1175–1196.
[42] G. Renversez, P. Boyer, A. Sagrini, Antiresonant reflecting optical waveguide microstructured fibers revisited: a new analysis based on leaky mode coupling, Opt. Express 14 (12) (2006) 5682–5687.
[43] L.G. Aio, A.M. Efimov, V.F. Kokorina, Refractive-index of chalcogenide glasses over a wide range of compositions, J. Non-Cryst. Solids 27 (3) (1978) 299–307.
[44] V.S. Shiryaev, J.L. Adam, X.H. Zhang, C. Boussard-Pledel, J. Lucas, M.F. Churbanov, Infrared fibers based on Te–As–Se glass system with low optical losses, J. Non-Cryst. Solids 336 (2) (2004) 113–119.
[45] F. Couny, F. Benabid, P.S. Light, Large-pitch kagome-structured hollow-core photonic crystal fiber, Opt. Lett. 31 (24) (2006) 3574–3576.

[46] Q. Coulombier, L. Brilland, P. Houizot, T. Chartier, T.-N. N'Guyen, F. Smektala, G. Renversez, A. Monteville, D. Méchin, T. Pain, H. Orain, J.-C. Sangleboeuf, J. Trolès, Casting method for low-loss chalcogenide microstructured optical fibers, Opt. Express 18 (9) (2010) 9107–9112.
[47] B.J. Mangan, L. Farr, A. Langford, P.J. Roberts, D.P. Williams, F. Couny, M. Lawman, M. Mason, S. Coupland, R. Flea, Low loss (1.7 dB/km) hollow core photonic bandgap fiber, in: Optical Fiber Communication Conference, 2004. OFC 2004 2.
[48] C.M. Smith, N. Venkataraman, M.T. Gallagher, D. Müller, J.A. West, N.F. Borrelli, D.C. Allan, K.W. Koch, Low-loss hollow-core silica/air photonic bandgap fibre, Nature 424 (6949) (2003) 657–659.